2021 43rd Annual International Conference of the
IEEE Engineering in Medicine & Biology Society (EMBC)
Oct 31 - Nov 4, 2021. Virtual Conference

Multi-Physical Tissue Modeling of a Human Urinary Bladder

Johannes Schüle[1], Franziska Krauß[1], Carina Veil[1], Stefanie Kunkel[1], Peter Somers[1], Cristina Tarín[1], and Oliver Sawodny[1]

***Abstract*— A multi-physical model of a human urinary bladder is an essential element for the potential application of electrical impedance spectroscopy during transurethral resection surgery, where measurements are taken at different fill levels inside the bladder. This work derives a multi-physical bladder tissue model that incorporates the electrical impedance properties with dependence on mechanical deformation due to filling of the bladder. The volume and ratio of the intracellular to extracellular tissue fluid heavily influence the electrical impedance characteristics and thus provide the connection between the mechanical and electrical domains. Modeling the fluid within the tissue links both the physical and histological processes and enables useful inferences of the properties from empiric observations. This is demonstrated by taking impedance measurements at different fill volumes. The resulting model provides a tool to analyze impedance measurements during surgery at different stress levels. In addition, this model can be used to determine patient-specific tissue parameters.**

I. Introduction

In the course of surgical interventions, tumorous tissue and its healthy environment must be differentiated. For this purpose, electrical impedance spectroscopy enables continuous measurements on living tissue to determine the pathologically induced changes in the tissue, since compressing tissue causes an increase in impedance. Consequently, impedance measurements also provide information about the mechanical properties that are characteristically related to the pathological changes. In order to make electrical impedance spectroscopy usable in a minimally invasive surgery through the urethra, it is essential to study the influence of mechanical stress on the impedance, since the bladder is repeatedly filled with liquid such as saline solution and, hence, expanded during the surgery.

From results found in literature, an increase in pressure applied externally on the tissue may have a more significant effect on the impedance measurement as any pathological changes [1], therefore, the mechanical impact has to be known in order to draw conclusions about the pathological changes. While the general impedance response of compressed tissue has been studied many times, the effect of strained tissue is largely unexplored. In this work an overall model is presented that establishes the link between the mechanical and electrical behavior of a urinary bladder. The focus lies on the behavior of the impedance under strain in order to differentiate the pathological changes from the mechanical changes due to the bladder filling.

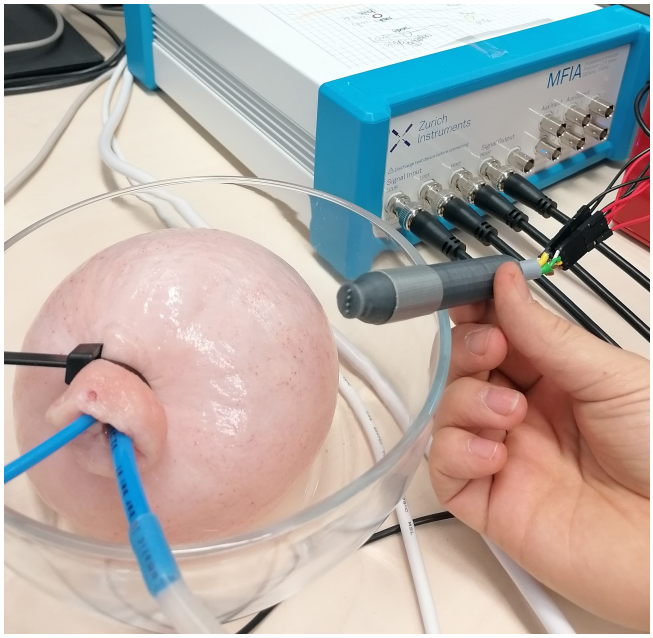

Fig. 1. A pig bladder turned inside out in order to measure the electrical impedance of the urothelium on the outer surface. The sensor for the impedance measurements has an inline electrode configuration. Two tubes, one for the pressure sensor and one for the water supply, were placed in the bladder and sealed off.

The bladder is divided into four tissue layers that have different characteristic properties. The innermost layer, consisting of a thin multi-cell layer urothelium isolates the urine from the underlying layers and helps fight infections and injuries. The remaining tissue layers are composed of a densely interwoven network of collagen and elastic fibers, which are primarily responsible for the elastic behavior of the bladder wall. A change of the bladder fill state directly leads to a change in the stress in the bladder wall. An increase in stress in the urothelium leads to an outflow of fluid at the cellular level. The displaced fluid originates both from the cells, passing through the cell membranes, and from the extracellular cavity. The intracellular and extracellular volumes largely determines the electrical behavior of tissue. A positive correlation between the amount of tissue fluid and the conductivity of the tissue at a certain frequency has been established in [2]: The greater the liquid content of the tissue, the more conductive it is. Similar results in [3]–[5] also evince that tissue with a high fluid density, such as muscle, has a higher conductivity than tissue with a low fluid

*This work was sponsored by the Graduate School 2543/1 "Intraoperative Multisensory Tissue Differentiation in Oncology" (project ID 40947457) funded by the German Research Foundation (DFG - Deutsche Forschungsgemeinschaft).

[1]Institute for System Dynamics, University of Stuttgart, 70563 Stuttgart, Germany {schuele, veil, somers, tarin, sawodny}@isys.uni-stuttgart.de

density, such as fat. Separate studies have also investigated the effect of externally applied pressure on the impedance of tissue [1], [6]–[8].

In this work, electrical behavior of tissue under compression is extended and modeled following the expansion process during filling of the the urinary bladder. The impedance measurements are performed on the inner wall of the bladder, because solely the urothelium, the innermost tissue layer, is of interest.

The paper is structured as follows. First, the mechanical model of the bladder is derived, which links the enclosed volume of the bladder to the mechanical stress of the bladder tissue wall. This is done condisdering the urothelium and the surrounding tissue layers as two separate entities. Consequently, the mechanical strain determines the volume change of the intracellular and extracellular cell volumes in the urothelium that is derived in the layer model. Subsequently, the electrical properties are modeled as a function of the extra and intracellular volumes to complete the overall model. The electrical model is fit to empiric observations, that were obtained from impedance measurements at different bladder fillings. The test setup can be seen in Figure 1.

II. Mechanical Stress-Strain Model

When filling, the tissue of the bladder exhibits a complex stress response in the wall, due to a combination of its non-linear elastic, viscous, and plastic mechanical properties and the active contraction of the bladder muscles [9]. As a result, the stress cannot be determined by a simple linear relation. The following non-linear model considers an empirical approach to describe the dependence between the stress in the bladder wall and the radius of the filling volume using test measurements. A hollow sphere with inner radius r and wall thickness h has proven to be a suitable description to approximate the form of the bladder [9]. This allows for modeling the bladder wall by a cut-out of the hollow sphere in the form of a cube of edge lengths λ_1, λ_2, and λ_3 on the coordinate axes x, y, and z, respectively. The orientation of the finite cuboid is illustrated in Figure 2.

The assumption of incompressible tissue has shown in [9]

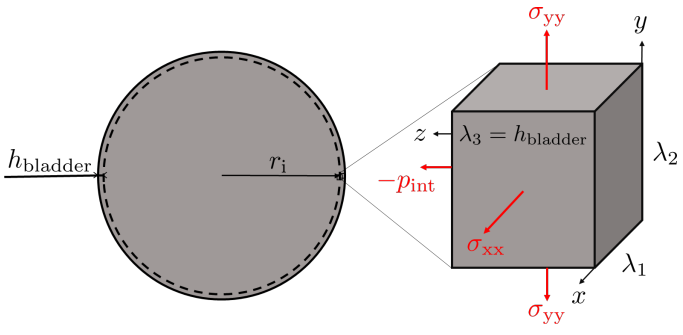

Fig. 2. Cuboidal cutout of the bladder wall with edge lengths λ_1, λ_2 and λ_3. and stresses σ_{xx}, σ_{yy} along the local coordinate axes.

to be a reasonable approach for modeling a rabbit mesentery, which exhibits similar stress-strain characteristics as considered in this work. When taking into account the compressed volume difference in proportion to the total tissue, it is found to be negligible [9]. Therefore, this assumption is used to model the stress-strain relationship, the incompressible volume of the cuboid bladder cutout is constant

$$V = \lambda_1 \lambda_2 \lambda_3 \equiv 1. \tag{1}$$

Since the identical stress $\sigma = \sigma_x = \sigma_y$ is present at the spherical bladder surface plane under internal pressure loading, the finite cuboid deforms equivalently in the x and y directions. The strain

$$\epsilon = \frac{\Delta l}{l_0} = \frac{l - l_0}{l_0} \tag{2}$$

of a material is defined by the ratio of the extension Δl and the initial length l_0. Whereas, the deformation is defined by the ratio

$$\lambda = \frac{l}{l_0} \tag{3}$$

which is assumed to increase equally in the xy surface plane resulting in $\lambda_1 = \lambda_2 = \lambda$. Combining this with (1), the bladder thickness can be written as $\lambda_3 = \frac{1}{\lambda^2}$. Hollow spheres with radius r and the wall thickness h are defined to be thin-walled, as soon as the condition

$$\frac{r}{h} > 10 \tag{4}$$

satisfies [10]. Considering a thin-walled sphere, Laplace's law relates the stress

$$\sigma = \frac{p_{\text{int}} r}{2h} \tag{5}$$

to the internal pressure p_{int}. The stress in the cutout is equivalently described by the inner radius

$$r = \lambda r_0 \tag{6}$$

with the initial inner radius r_0, the wall thickness

$$h = \frac{1}{\lambda^2} h_0, \tag{7}$$

and the internal pressure, resulting in

$$\sigma = \frac{p_{\text{int}} r_0}{2h_0} \lambda^3 = q\lambda^3 \tag{8}$$

with the pressure component q and the strain ratio λ. The stress in the bladder wall increases exponentially with an increasing strain due to adjustments in the collagen structure as well as to contractile elements. The corresponding measurement data is analyzed and shown in Figure (3), where the measured characteristic can be approximated by the differential trial function

$$\frac{\delta q}{\delta \lambda} = -aq + b. \tag{9}$$

Considering the boundary condition $q(\lambda^\star) = q^*$ at a certain measured strain ratio $\lambda = \lambda^*$ the solution of (9) with (8) provides the unique stress model

$$\sigma(\lambda) = \frac{b - e^{-a\lambda}(be^{a\lambda^*} - aq^* e^{a\lambda^*})}{a} \lambda^3. \tag{10}$$

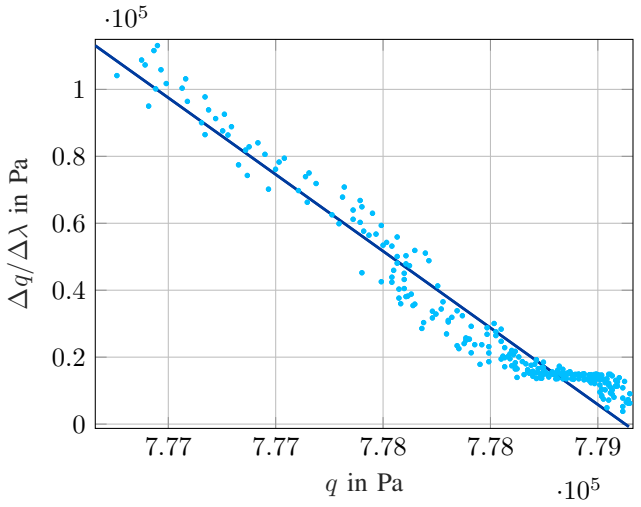

Fig. 3. Representation of $\Delta q/\Delta\lambda$ over q. The parameterization (—) is a good approximation of the measured values (····).

III. Urothelial Tissue Fluid Model

The extra- and intracellular volume links the mechanical and electrical model. For the impedance measurements, the electrical current flows mostly through the urothelium, therefore, its tissue composition is decisive for the resulting model parameters of the electrical model. Due to this, it is necessary to investigate how much fluid is displaced from the urothelium while the bladder is being filled.

A. Internal Tissue Fluid Model

The empirically determined Darcy's law

$$\dot{\mathrm{q}} = \frac{Q}{A} = K \cdot \nabla P \tag{11}$$

provides a reliable model of the fluid dispersion flow $\dot{\mathrm{q}}$ through a medium, such as tissue, by describing the correlation between the dispersed volume flow Q through a considered unit area A of the membrane by a constant hydraulic conductivity K and the intermediate pressure gradient ∇P [11], [12]. According to (1), the steady state of the pressure obeys Laplace's equation

$$\nabla^2 P = 0, \tag{12}$$

the pressure gradient

$$\nabla P = \frac{(p_{\text{uro}} - p_{\text{int}})}{r \ln(\frac{r+h_{\text{uro}}}{r})} \tag{13}$$

between the inner wall of the bladder and the outermost layer of the urothelium can be related to the urothelium thickness h_{uro}, the bladder wall thickness h, the internal pressure p_{int}, and the pressure p_{uro} at the boundary between the urothelium and the remaining layers. For simplicity, the parameters that are related to the urothelium are indicated by the subscript 'uro'; correspondingly, parameters that indicate the dependencies of the muscle are characterized by the subscript 'mus'. From (11) follows the relation

$$\dot{\mathrm{q}} = K \frac{(p_{\text{uro}} - p_{\text{int}})}{r \ln(\frac{r+h_{\text{uro}}}{r})} \tag{14}$$

for volume flow Q per area A. As the bladder expands, the fluid can dissipate through the surface area

$$O = 4\pi(r + h_{\text{uro}})^2 \tag{15}$$

of the urothelium. Using (11) and (15), the volume change of the urothelium is determined by

$$\frac{dV_{\text{uro}}}{dt} = \dot{\mathrm{q}} O = K \frac{p_{\text{uro}} - p_{\text{int}}}{\ln(\frac{r+h_{\text{uro}}}{r})} 4\pi(r + h_{\text{uro}}). \tag{16}$$

Depending on r, the thickness of the bladder wall

$$h = \sqrt[3]{r^3 + \frac{3}{4\pi} V_{\text{tis}}} - r \tag{17}$$

is calculated from the incompressible overall tissue volume V_{tis}.

B. Link of Tissue Fluid to Stress-Strain Model

Since the bladder wall is considered to be an orthotropic material, loads in the transverse xy directions cause the same tissue reaction in the bladder cutout. The stress-strain relations for a linear orthotropic tissue model results in the matrix representation

$$\begin{bmatrix} \epsilon_{xx} \\ \epsilon_{yy} \\ \epsilon_{zz} \end{bmatrix} = \begin{bmatrix} \frac{1}{E} & -\frac{v}{E} & -\frac{v_z}{E_z} \\ -\frac{v}{E} & \frac{1}{E} & -\frac{v_z}{E_z} \\ -\frac{v}{E} & -\frac{v}{E} & \frac{1}{E_{zx}} \end{bmatrix} \begin{bmatrix} \sigma_{xx} \\ \sigma_{yy} \\ \sigma_{zz} \end{bmatrix} \tag{18}$$

with an uniform Poisson's ratio v in the surface plane and v_z in the radial z-direction. Shear stresses are neglected as the dominating loading comes from the induced hoop stress, hence $\sigma_{yz} = \sigma_{zx} = \sigma_{xy} = 0$ [13]–[15].

Several parameters are necessary to specify the strain response. Since this model does not investigate the stress curves in the xy plane of the cutout, but rather the pressures and strains in the radial z-direction, fixed elasticity moduli are used. Depending on the direction of loading, the Young's modulus

$$E_i = \frac{\sigma_i}{\epsilon_i} \tag{19}$$

is determined by dividing the stress by the strain in the considered direction i. Figure 2 illustrates the stresses on the bladder cutout: the modified hoop stress σ described in (10) acts in the xy plane, whereas p_{int} acts in the negative z direction. Described by (18) with use of (10) and (19) exploited in the z-direction, the cutout is deformed equally with

$$\epsilon = \frac{1 - v}{E} \sigma(\lambda) + \frac{v_z}{E_z} p_{\text{int}} \tag{20}$$

in both the x- and y-direction and in the z-direction it is deformed according to

$$\epsilon_{zz} = -2\frac{v_z}{E} \sigma(\lambda) - \frac{1}{E_z} p_{\text{int}}. \tag{21}$$

This behavior of the urothelium is analyzed separately from the rest of the bladder wall. Since the muscle in the bladder composes a large portion of the volume, the remaining portion is designated as the muscle layer for the sake of simplicity. The interlayer coupling causes the tissue layers to elongate similarly with $\epsilon_{\text{uro}} = \epsilon_{\text{muscle}}$, where the strains are determined by

$$\epsilon_{\text{uro}} = \frac{1 - v_{\text{uro}}}{E_{\text{uro}}}\sigma_{\text{uro}} + \frac{v_{z,\text{uro}}}{E_{z,\text{uro}}}p_{\text{int}} \tag{22}$$

and

$$\epsilon_{\text{mus}} = \frac{1 - v_{\text{mus}}}{E_{\text{mus}}}\sigma_{\text{muscle}} + \frac{v_{z,\text{mus}}}{E_{z,\text{mus}}}p_{\text{uro}}. \tag{23}$$

For this reason, the total stress $\sigma(\lambda)$ in the bladder wall as described in (10) can be separated into two components: the stress in the urothelium and the stress in the muscle $\sigma(\lambda) = \sigma_{\text{uro}}(\lambda) + \sigma_{\text{muscle}}(\lambda)$. The pressure p_{int} and stress σ_{uro} act on the urothelium, whereas the pressure p_{uro} and stress σ_{mus} act on the muscle layer. Using (22) and (23), the stress $\sigma_{\text{mus}} = \sigma - \sigma_{\text{uro}}$ can be used to determine the pressure

$$\begin{aligned} p_{\text{uro}} = &\left(\frac{1 - v_{\text{uro}}}{E_{\text{uro}}}\sigma_{\text{uro}} + \frac{v_{z,\text{uro}}}{E_{z,\text{uro}}}p_{\text{int}}\right)\frac{E_{z,\text{mus}}}{v_{z,\text{mus}}} \\ &+ \frac{1 - v_{\text{mus}}}{E_{\text{mus}}}\left(\sigma_{\text{uro}} - \sigma\right)\frac{E_{z,\text{mus}}}{v_{z,\text{mus}}} \end{aligned} \tag{24}$$

that acts at the boundary between urothelium and the muscle layer. The stress in the urothelium is determined by the change in its thickness. Considering (21), the strain of the urothelium in z direction is modeled by

$$\epsilon_{z,\text{uro}} = -2\frac{v_{z,\text{uro}}}{E_{\text{uro}}}\sigma_{\text{uro}} - \frac{1}{E_{z\text{uro}}}p_{\text{int}}. \tag{25}$$

According to this, the stress in the urothelium

$$\sigma_{\text{uro}} = -\frac{E_{\text{uro}}}{2v_{z,\text{uro}}}(\epsilon_{z,\text{uro}} + \frac{p_{\text{int}}}{E_{z,\text{uro}}}) \tag{26}$$

depends on the strain of the urothelium. Where the wall thickness of the urothelium

$$h_{\text{uro}} = \sqrt[3]{r^3 + \frac{3}{4\pi}V_{\text{uro}}} - r \tag{27}$$

is determined by the volume of the urothelium that results from (16) and in this manner the dynamic model is fully defined using an initial condition for the initial urthelium tissue volume.

C. Modeling of the Electrical Tissue Properties

The impedance of tissue depends on its structure and current load conditions. In general, the conductivity of tissue depends on the ion concentration and ion mobility [16]. The electrical conductivity σ_{el} describes a material's ability to transport electric charges. The ability to intercept or hold charges and rotate molecular dipoles is defined as the material permittivity ε_{el} [16], [17]. For tissues, the material parameters σ_{el} and ε_{el} are not constant, but vary with the frequency of the applied electric field. This behavior is in accordance with the pathological understanding: at low frequencies, the dipoles can still align according to the changing field, which corresponds to a high permittivity. As a result, charge carriers are forced to move long distances at a low frequency. This increases the probability of being absorbed in other tissue elements. As the frequency increases, the dipoles cannot follow the alternating field and the permittivity falls. At the same time, the charge carriers have to cover shorter distances and are trapped less likely. As a result, the conductivity increases [17]. This simultaneous increase of conductivity and decrease of permittivity in a certain frequency range are referred to as dispersion

The Cole-Cole equation for the impedance

$$Z = R_\infty + \frac{R_0 - R_\infty}{1 + (\frac{jf}{f_c})^\alpha} \tag{28}$$

provides a powerful tool to model this effect in the frequency spectrum, where α is a specific material constant of the tissue dispersion. A well-established electrical equivalent circuit that models the electrical behavior of tissue, at a constant stress strain level is shown in Figure 4. Here, the impedance is described by

$$Z = \left[\frac{1}{R_{\text{ext}}} + \frac{1}{R_{\text{int}} + \frac{1}{j\omega C_{\text{m}}}}\right]^{-1}, \tag{29}$$

where the resistances R_{int} and R_{ext} respectively model the intracellular and extracellular conductances, and the capacitor C_{m} determines the capacitive behavior of the cell membrane [18].

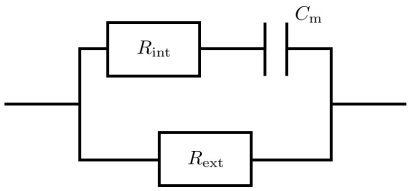

Fig. 4. Representative electrical circuit equivalence for tissue.

IV. Experimental Impedance Measurements

For data acquisition, correlation analysis and modeling, a series of measurements on a total number of four individual pig bladders were conducted. The bladders are taken from fresh pig cadavers provided by the Urology Clinic in Tübingen, Germany. A picture of the test setup is shown in Figure 1. In general, pig urinary bladders are a good representative of the human urinary bladder in terms of their anatomical and especially, histological nature [6]. Therefore, the measured data and empirical correlations can be generalized qualitatively to the human bladder. For the measurements, the pig bladders were turned inside out and, before they were sealed, a pressure sensor and supply tube were inserted. As a result, the electrical characteristics of the epithelium could be measured externally using an impedance analyzer and a laboratory pump controlled the bladder fill volume via the supply tube. As seen in Figure 5, the impedance measurements are consistent with literature for pressurized tissue [7]. As the fill volume and stress-strain level in the bladder wall increases, the resistances are also

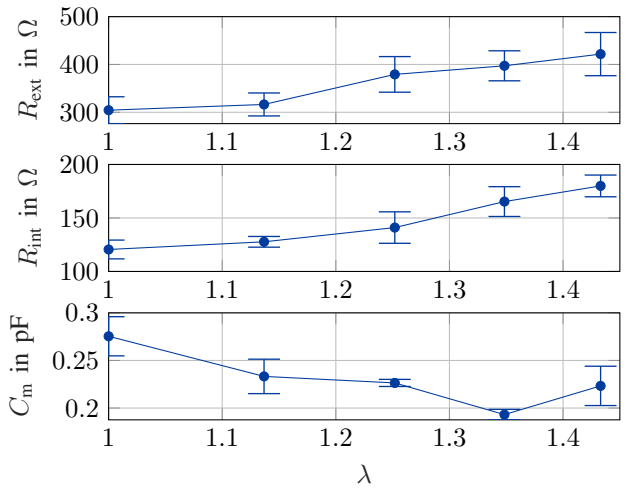

Fig. 5. Analyzed measurement results of four independent pig bladders. Extracellular resistance, intracellular resistance, and membrane capacitance as a function of volume expansion λ.

increasing. Simultaneously, the capacity of the cell membrane decreases. For a compression load, this characteristic is discussed in the literature through the tissue fluid. If the fluid is displaced, this is followed by a decrease in conductivity and an increase in resistance. This phenomenon is observed equally for both, the extracellular and intracellular resistances. Taking the measurements, the upfront identification is given by the courses of the resistance R_0 at low frequency $f \to 0$, the resistance R_∞ for $f \to \infty$, and α is freely chosen to maximize the fit of (28) the to the measurements of (29). As a result, the necessary parameters for (29) can be determined from (28). At low frequency $f \to 0$, the capacitor charges and blocks current through the cell while all current is conducted by the extracellular matrix through R_{ext}.

A. Dependency to the Intracellular and Extracellular Volume

The coupling between the strain and the intracellular volume is established by the empirical model via the relation of the electrical properties R_{int} and C_m to the extension λ. The measured impedance data, shown in Figure 5, were taken and analyzed related to a specific sensor geometry. The intracellular volume V_{int} and extracellular volume V_{ext} are considered in the following as the effective sum over the individual cell volumes of the measured sensor area. Based on the derivation of the pathological correlations between the intra-/ extracellular volumes and the electrical characteristics is determined empirically using an optimization-based grey box regression. For this purpose, the intracellular volume is coupled with the the intracellular resistance and the membrane capacitance. The model selection is made based on histologically justifiable correlations, as well as on the available measurement data. The impedance measurements were normalized with respect to resistance $R_{int,0}$ and capacitance $C_{m,0}$ of an unfilled bladder and the following model structures

$$\tilde{R}_{int} = \frac{R_{int}}{R_{int,0}} = (1 + \frac{\varsigma_{int}(\lambda - 1)}{V_{int,0} - \varsigma_{int}(\lambda - 1)}) \tag{30}$$

and

$$\tilde{C}_m = \frac{C_m}{C_{m,0}} = \frac{\varsigma_{int}(\lambda - 1)}{V_{int,0}} \tag{31}$$

are proposed. Here, ς_{int} is an intracellular volume related conductivity and permittivity coefficient. The solution of parameterization $p_e = [V_{int,0}, \varsigma_{int}, \tilde{R}_{int,0}]$ for the trial functions (30) and (31) is provided by a least-square regression on the n measured sample points, shown in Figure 5. Accordingly, the model

$$\tilde{R}_{ext} = \frac{R_{ext}}{R_{ext,0}} = (1 + \frac{\varsigma_{ext}(\lambda - 1)}{V_{ext,0} - \varsigma_{ext}(\lambda - 1)}) \tag{32}$$

for extracellular resistance is constructed with the parameterization $p_e = [V_{ext,0}, \varsigma_{int}, \tilde{R}_{ext,0}]$. Since V_{uro} is already given via (16) and $V_{ext} = V_{uro} - V_{int}$, only the extracellular conductivity coefficient ς_{ext} has to be identified by using the measurement data of the extracellular resistance. Nevertheless, the least-square optimization and measurement data can be further exploited to identify unknown parameters of the mechanical model since V_{uro} links all mechanical submodels into the optimization problem.

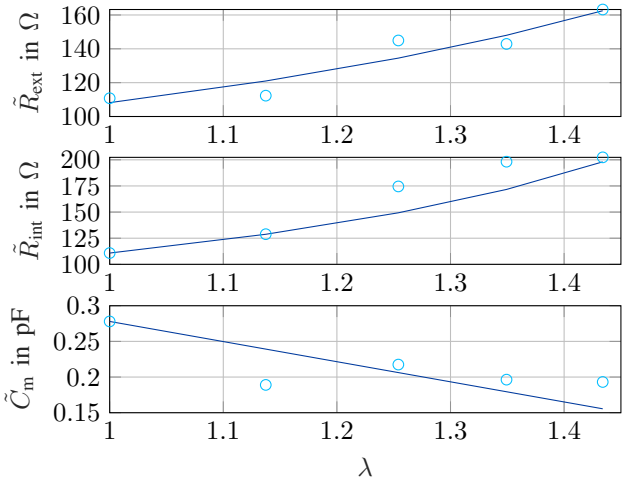

Fig. 6. Intracellular and extracellular space over the deformation ratio λ with the measured data (O) and the fitted curve (—).

B. Results of the Empirical Model

In Table I the parameterization of the regression problem is listed. The obtained values for $V_{int,0}$ and ς_{int} are in accordance with the literature in a plausible range.
Along with the results in Table I and the solutions of the regression, the regressed prediction is shown in Figure 6.

The regression corresponds to a satisfactory approximation, as there are no significant deviations between the modeled curve and the measurements.

TABLE I

EMPIRICAL MODEL PARAMETERS FOR 4 TEST BLADDERS

Nr	$V_{\text{int},0}$ [m^3]	ς_{int} [m^3]	$\tilde{R}_{\text{int},0}$ [Ω]	$\tilde{C}_{\text{m},0}$ [pF]	$\tilde{R}_{\text{ext},0}$ [Ω]
1	$1.05 \cdot \mathbf{e}^{-8}$	$8.50 \cdot \mathbf{e}^{-9}$	0.93	0.93	2.53
2	$1.75 \cdot \mathbf{e}^{-8}$	$6.40 \cdot \mathbf{e}^{-9}$	0.94	1.05	2.31
3	$9.92 \cdot \mathbf{e}^{-9}$	$1.10 \cdot \mathbf{e}^{-8}$	1	1	3.13
4	$1.99 \cdot \mathbf{e}^{-7}$	$9.35 \cdot \mathbf{e}^{-8}$	1.44	0.69	2.8

V. CONCLUSION

The presented model includes the mechanical states and the electrical states of a urinary bladder as a function of the filling volume, which is determined from both the analytical relations and empirical correlations. In an experimental setup, measurements were taken, evaluated and considered in the model derivation. This model provides a method to normalize the effect of the mechanical stress strain on the impedance of the urothelium through a correlation of cellular volume and electrical properties. This allows first approaches for tissue classification using impedance spectroscopy for measurement data taken at different stress-strain levels on an urinary bladder. The derived model equations and correlations also allow for generating synthetic measurement data, which can be used to build and develop intelligent data-driven algorithms to classify impedance measurements.

REFERENCES

[1] C.-A. Gonzalez-Correa, B. Brown *et al.*, "Electrical bioimpedance readings increase with higher pressure applied to the measuring probe," *Physiological measurement*, vol. 26, pp. S39–47, 05 2005.

[2] S. R. Smith and K. R. Foster, "Dielectric properties of low-water-content tissues," *Physics in Medicine and Biology*, vol. 30, no. 9, pp. 965–973, sep 1985.

[3] S. Gabriel, R. W. Lau, and C. Gabriel, "The dielectric properties of biological tissues: III. parametric models for the dielectric spectrum of tissues," *Physics in Medicine and Biology*, vol. 41, no. 11, pp. 2271–2293, nov 1996.

[4] C. Gabriel, S. Gabriel, and E. Corthout, "The dielectric properties of biological tissues: I. literature survey," *Physics in Medicine and Biology*, vol. 41, no. 11, pp. 2231–2249, nov 1996.

[5] S. Gabriel, R. W. Lau, and C. Gabriel, "The dielectric properties of biological tissues: II. measurements in the frequency range 10 hz to 20 GHz," *Physics in Medicine and Biology*, vol. 41, no. 11, pp. 2251–2269, nov 1996.

[6] A. Keshtkar and A. Keshtkar, "The effect of applied pressure on the electrical impedance of the bladder tissue using small and large probes," *Journal of medical engineering & technology*, vol. 32, no. 6, pp. 505–511, 2008.

[7] R. Dodde, J. Bull, and A. Shih, "Bioimpedance of soft tissue under compression," *Physiological measurement*, vol. 33, no. 6, p. 1095, 2012.

[8] S. M. Moqadam, P. Grewal *et al.*, "Compression-dependency of soft tissue bioimpedance for in-vivo and in-vitro tissue testing," *Journal of Electrical Bioimpedance*, vol. 6, no. 1, pp. 22–32, 2015.

[9] S. Korossis, F. Bolland *et al.*, "Regional biomechanical and histological characterisation of the passive porcine urinary bladder: Implications for augmentation and tissue engineering strategies," *Biomaterials*, vol. 30, no. 2, pp. 266 – 275, 2009.

[10] G. Sinclair and J. Helms, "A review of simple formulae for elastic hoop stresses in cylindrical and spherical pressure vessels: What can be used when," *International Journal of Pressure Vessels and Piping*, vol. 128, pp. 1 – 7, 2015.

[11] M. Intaglietta and E. de Plomb, "Fluid exchange in tunnel and tube capillaries," *Microvascular Research*, vol. 6, no. 2, pp. 153 – 168, 1973.

[12] N. P. Reddy, G. V. B. Cochran, and T. A. Krouskop, "Interstitial fluid flow as a factor in decubitus ulcer formation," *Journal of Biomechanics*, vol. 14, no. 12, pp. 879 – 881, 1981.

[13] H. Altenbach, *Kontinuumsmechanik*. Springer, 2012.

[14] A. P. Boresi, R. J. Schmidt *et al.*, *Advanced mechanics of materials*. Wiley New York, 1985, vol. 6.

[15] F. A. Duck, "Mechanical properties of tissue - chapter 5," in *Physical Properties of Tissues*, F. A. Duck, Ed. London: Academic Press, 1990, pp. 137 – 165.

[16] D. A. Dean, T. Ramanathan *et al.*, "Electrical impedance spectroscopy study of biological tissues." *Journal of electrostatics*, vol. 66, pp. 165–177, Mar 2008.

[17] D. Miklavčič, N. Pavšelj, and F. X. Hart, *Electric Properties of Tissues*. American Cancer Society, 2006.

[18] F. Thiel, "Bioimpedanz-analysator zur nichtinvasiven funktions- und zustandsanalyse von organen und gewebe." 03 2003.